Macromolecules

Article

Cite This: Macromolecules 2019, 52, 8759−8770

pubs.acs.org/Macromolecules

# Invertible Micelles Based on Ion-Specific Interactions of $Sr^{2+}$ and $Ba^{2+}$ with Double Anionic Block Copolyelectrolytes

Nico Carl,[†,‡] Sylvain Prévost,[†] Ralf Schweins,[†] Judith E. Houston,[§] Isabelle Morfin,[∥] and Klaus Huber*[,‡]

[†]Large Scale Structures Group, DS, Institut Laue-Langevin, 71 Avenue des Martyrs, CS 20 156, 38042 Grenoble, France

[‡]Chemistry Departement, University of Paderborn, Warburger Str. 100, 33098 Paderborn, North Rhine-Westphalia, Germany

[§]Jülich Centre for Neutron Science, Forschungszentrum Jülich GmbH, 85747 Garching, Bavaria, Germany

[∥]Université Grenoble Alpes, LiPhy, 38000 Grenoble, France

Supporting Information

**ABSTRACT:** Polyelectrolytes show diverse ion-specific effects with a wide variety of ions. In the present work, we study the solution behavior of diblock copolymers with polyacrylate (PA) and polystyrenesulfonate (PSS) blocks in the presence of the earth alkaline cations $Ca^{2+}$, $Sr^{2+}$, and $Ba^{2+}$. Micellization can be triggered by a variation in temperature. For $Ca^{2+}$, this micelle formation occurs at high temperatures, while for $Sr^{2+}$ and $Ba^{2+}$, it occurs at high and low temperatures with an intermediate temperature regime of single chains. Small-angle neutron scattering on a partly deuterated block copolymer unambiguously revealed that at low temperatures, PSS/$M^{2+}$ forms the core of the micelles, whereas at high temperatures, PA/$M^{2+}$ forms the core, effectively allowing to reverse the micelle structure by changing the temperature. This inversion of the micellar morphology, induced by a dual-responsive behavior, can be understood by using isothermal titration calorimetry and elucidating the thermodynamics of cation binding.

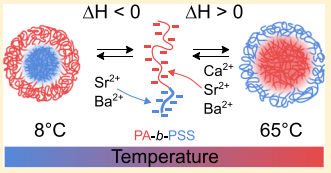


## INTRODUCTION

Amphiphilic block copolymers self-assemble into structures ranging from spherical[1] to worm-like micelles[2] or vesicles.[3] Extensive research has been conducted to develop block copolymers where one of the blocks responds to external stimuli such as temperature,[4] pH,[5] pressure,[6] or light[7] in order to affect the hydrophobicity of the respective block and hence to switch between the monomeric and self-assembled state. So far, such stimuli or combinations thereof have been used to generate switchable emulsifiers,[8] to control rheology[9] or to release active agents.[10] In order to create even more versatile systems, research efforts were aiming at block copolymers where each of the two blocks responds to a different stimulus. Such systems were expected to accomplish an inversion of the micellar structure by reversibly addressing the stimulus of the two blocks one by one. Accordingly, the term schizophrenic micelles has been coined for these systems.[11,12,12−19]

The underlying concept of many of such systems makes use of one block with an upper critical solution temperature (UCST) and a second block with a lower critical solution temperature (LCST). Furthermore, it is ensured that a significant temperature gap exists between the UCST and LCST.[11] Only such a gap makes accessible the state of single block copolymer chains in between the state of micelles and of inverted micelles.[11] However, a problem observed during those efforts was that in the regime, where both blocks should be soluble the chains tend to aggregate.[11,17,18] In the light of potential applications such as the controlled uptake, transport, or release of low-molecular weight compounds, these effects are undesirable as they might provide cavities which keep back the cargo and prevent the complete release of it.

In the present work, we pursue a slightly different strategy to realize such an invertible system. Block copolymers of two negatively charged polyelectrolytes, sodium polyacrylate (PA) and sodium polystyrene sulphonate (PSS), are synthesized.[20,21] Polyelectrolytes are commonly used as building blocks for block copolymers because of their water solubility, pH responsivity, and the ability to form charge-stabilized self-assembled structures.[1,22,23] The selection of PA and PSS is based on previous works,[24−26] which demonstrated unambiguously that the two polyanions interact specifically and in a different manner with alkaline earth cations. This interaction is temperature-dependent, whereby the temperature dependence also differs when going from PA to PSS.[24,26]

In more detail, earth alkaline metal cations $M^{2+}$ complex the anionic moieties of PA and neutralize the negative charges. This results in phase separation of the polymer at a critical concentration of $[M^{2+}]_c$, which depends on the PA concentration [PA][25,27]

$$[M^{2+}]_c = r_0 + m[PA] \quad (1)$$

with [PA] being the concentration of PA monomer units, $r_0$ being the minimum concentration of $M^{2+}$ required for precipitation and $m$ being the stoichiometry of binding.

Received: September 13, 2019
Revised: October 22, 2019
Published: November 8, 2019






DOI: 10.1021/acs.macromol.9b01924
Macromolecules 2019, 52, 8759−8770

Strikingly, the binding of $M^{2+}$ to PA is endothermic with all three cations,[26,28,29] and phase separation is thus promoted by an increase of temperature,[26] discernible in a decrease in $r_0$ with an increase of temperature.

In contrast, PSS shows a completely different phase behavior with earth alkaline cations. No macroscopic phase separation is observed in the presence of $Ca^{2+}$ and $Sr^{2+}$.[24,29] For $Ba^{2+}$, a horizontal phase boundary according to

$$[Ba^{2+}]_c = r_0 \quad (2)$$

is observed.[24,30,31] Above all, the binding of $Ba^{2+}$ to the anionic moieties of PSS is dominated by an exothermic complexation[29] and $r_0$ decreases in this case with decreasing temperature.[24]

We deliberately used the term phase separation instead of precipitation for all these cases as we are most likely dealing with a liquid−liquid phase separation (LLPS) of the dissolved polyelectrolytes neutralized via specific interactions with alkaline earth cations.[32] In fact Kanai and Muthukumar[33] could demonstrate that the LLPS observed with $Ba^{2+}$ and PSS obeys an UCST behavior. As the impact of temperature on the binding of $Ba^{2+}$ to PA is inverse to the binding of $Ba^{2+}$ to PSS, we have a good reason to assume that the interaction with $Ba^{2+}$ exhibits a LCST. Given that the interaction of PA with $M^{2+}$ obeys a LCST behavior, whereas the interaction of PSS with $Ba^{2+}$ is of an UCST type, a combination of these two features in a block copolyelectrolyte may pave the road to invertible micelles with $Ba^{2+}$ and PA-*b*-PSS diblock copolymers, in analogy to the concept pursued by Papadakis et al.[11,17,18] It is this idea, which is at the center of the present work. A first step along this line has already been accomplished in a preceding work, in which we showed that these differing modes of interaction with $Ca^{2+}$ can be used to self-assemble PA-*b*-PSS block copolymers into well-defined micelles.[20]

Herein, we report on the effect of temperature on the self-assembly of PA-*b*-PSS in the presence of $Ca^{2+}$, $Sr^{2+}$, and $Ba^{2+}$. Small-angle neutron scattering (SANS) in combination with isothermal titration calorimetry (ITC) is employed to unambiguously prove that it is possible to create an invertible system with this type of block copolymer and that the inversion of the micelle structure passes a regime of single chains. At the same time, the present results introduce multivalent cations in combination with block copolyelectrolytes as a new toolbox for temperature-responsive polymers and dual-responsive systems.

## EXPERIMENTS AND DATA ANALYSIS

**Materials.** Light water was purified using a Milli-Q-system; heavy water ($D_2O$, Euriso-top, France, 99.90 at. % deuterium) was filtered with a 100 nm PVDF filter (Merck Millex MPSLVV033RS) prior to use. $CaCl_2{\cdot}2H_2O$ (Sigma-Aldrich, France, >99.9%), $SrCl_2{\cdot}6H_2O$ (Fluka, Germany, >99%), $BaCl_2{\cdot}2H_2O$ (Sigma-Aldrich, Germany, >99.999%), NaCl (Sigma-Aldrich, France, >99.9%), and NaOH (Sigma-Aldrich, France) were used as received.

**Polymer Synthesis.** The synthesis of the (block) copolymers was done using reversible addition−fragmentation chain-transfer polymerization and is described in detail in the Supporting Information. The investigated PA-*b*-PSS block copolymers have a block ratio of PA to PSS of 94:6.

**Sample Preparation.** In general, the samples were prepared according to a previously suggested approach. The concentration of positive charges is kept constant at 100 mmol $L^{-1}$. In order to achieve this, the solvent contains 100 mmol $L^{-1}$ NaCl and $M^{2+}$ cations are added by replacing a certain amount of 100 mmol $L^{-1}$ NaCl by the corresponding amount of solution of $MCl_2$.

For the scattering experiments, first, an aqueous stock solution of the freeze-dried polymer in 100 mmol $L^{-1}$ NaCl was prepared at a polymer concentration of 8 g $L^{-1}$ and adjusted to pH of 9 using a 100 mmol $L^{-1}$ NaOH solution. The solution is filled up with 100 mmol $L^{-1}$ NaCl solution and the desired amount of 100 mmol $L^{-1}$ $CaCl_2$ ($SrCl_2$/$BaCl_2$) by dropwise addition under vigorous stirring. The final polymer concentration was 1 or 4 g $L^{-1}$.

The samples for small-angle X-ray scattering (SAXS) and ITC were prepared in $H_2O$; otherwise, the samples were prepared in $D_2O$ or a mixture of $H_2O$ and $D_2O$.

**Density Measurements.** The density of the sodium salt of PA and PSS was measured using a DSA 5000 M densitometer (Anton-Paar) in a temperature range from 5 to 65 °C. Details can be found in the Supporting Information.

**Small-Angle Neutron Scattering.** Small-angle neutron scattering (SANS) measurements were performed at the D11 SANS instrument of the Institut Laue-Langevin (Grenoble, France). Three sample-to-detector distances (39.0 m collimation 40.5, 8.0 m collimation 8.0, and 1.4 m collimation 5.5 m) and a neutron wavelength of 0.5 nm (full width at half-maximum 9%) were used to cover a $q$-range of $2 \times 10^{-2}$ to 5 $nm^{-1}$. We used a circular neutron beam with a diameter of 15 mm. Scattered neutrons were detected with a $^3$He MWPC detector (CERCA) with 256 × 256 pixels of 3.75 mm × 3.75 mm pixel size. The detector images were azimuthally averaged, corrected to transmission of the direct beam, and scaled to absolute intensity using the LAMP software. A 1 mm $H_2O$ cell ($d\Sigma/d\Omega$ = 0.929 $cm^{-1}$) served as secondary calibration standard. The incoherent background and the scattering from the solvent were subtracted from the scattering curves. Details for the data reduction can be found in Chapter 2 of ref 34. The sample temperature was adjusted to values between 6 to 65 °C using a circulating water bath.

Additional SANS measurements were performed at the KWS2 small-angle scattering instrument of the Heinz Maier-Leibnitz Zentrum (Garching, Germany).[35] Three sample-to-detector distances (19.6 m collimation 20.0 m $\lambda$ = 10 Å, 7.7 m collimation 8.0 m $\lambda$ = 5 Å, 1.7 m collimation 2.0 m $\lambda$ = 5 Å) were used to cover a $q$-range of $3 \times 10^{-2}$ to 1.0 $nm^{-1}$. Scattered neutrons were detected with a $^3$He multitube detector (GE Reuter Stokes Inc).[36] The detector images were azimuthally averaged, corrected to transmission of the direct beam, and scaled to absolute intensity of plexiglass as the secondary calibration standard using the QtiKWS software. The incoherent background and the scattering from the solvent were subtracted from the scattering curves.

**Small-Angle X-ray Scattering.** SAXS experiments were performed at the ID02 beamline of the European Synchrotron Radiation Facility (ESRF). Two sample-to-detector distances (10 and 1 m) were measured at an X-ray energy of 12.46 keV (0.0995 nm) using a Rayonix MX-170HS CCD detector to cover a $q$-range of $8 \times 10^{-3}$ to 6 $nm^{-1}$.

Additional SAXS data were obtained from the D2AM beamline of the ESRF. Two sample-to-detector distances (2.2 and 0.6 m) were measured at an X-ray energy of 16.00 keV (0.0775 nm) using a XPAD-D5 hybrid pixel detector to cover a $q$-range of $5 \times 10^{-2}$ to 7 $nm^{-1}$.

Samples were filled in a 2 mm flow-through quartz glass capillary (WJM Glas Müller, Berlin, Germany) to facilitate accurate background subtraction. The detector images were corrected for dark and flat-field, azimuthally averaged, and corrected to transmission of the direct beam. The data were scaled to absolute intensity using water as a secondary standard.[37,38] Error bars were estimated assuming Poisson statistics.

**Static and Dynamic Light Scattering.** Static and dynamic light scattering (SLS, DLS) available in the ILL PSCM lab were performed using an ALV CGS-3 (ALV, Langen, Germany) equipped with a HeNe laser operating at $\lambda_0$ = 632.8 nm. The samples were filtered in cylindrical quartz glass cells using Millex PDVF filters with a pore size of 0.45 $\mu$m. SLS and DLS were measured simultaneously in an angular range from 30 to 150° in steps of 10 °C at temperatures ranging from 6 to 65 °C.



DOI: 10.1021/acs.macromol.9b01924
Macromolecules 2019, 52, 8759−8770

The intensity−time correlation function $g_2(\tau) - 1$ measured with DLS was analyzed using the method of cumulants[39]

$$g_2(\tau) - 1 = \beta \exp(-2\Gamma\tau)\left(1 + \frac{\mu_2}{2!}\tau^2\right)^2 \quad (3)$$

$\beta$ is a factor, which depends on the experimental setup, $\Gamma$ is the relaxation rate, and $\mu_2$ is the second cumulant. The apparent diffusion coefficient $D_{app}(c,q)$ for a given $q$ is calculated according to

$$D_{app} = \frac{\Gamma}{q^2} \quad (4)$$

The diffusion coefficient is extrapolated toward $q = 0$ and where applicable, to $c = 0$ according to[40,41]

$$D_{app}(c, q) = D_0(1 + CR_g^2q^2 + k_Dc) \quad (5)$$

where $C$ and $k_D$ are constants describing $q$ and the concentration dependence of $D_{app}$, respectively. The diffusion coefficient $D_0$ is used to calculate the hydrodynamic radius $R_h$ using the Stokes−Einstein equation

$$R_h = \frac{k_BT}{6\pi\eta D_0} \quad (6)$$

where $T$ is the temperature, $k_B$ is the Boltzmann constant, and $\eta$ the viscosity of the solvent. The temperature-dependent viscosity of $D_2O$, which differs from that of $H_2O$, was obtained from ref 42.

Static light scattering was evaluated with the Zimm equation[43]

$$\frac{Kc}{\Delta R_\theta} = \frac{1}{M_w} + 2A_2c + \frac{R_g^2}{3M_w}q^2 \quad (7)$$

where $c$ is the mass concentration of the polymer, $M_w$ is the weight-averaged molar mass of the polymer, $A_2$ is the second osmotic virial coefficient, and $R_g$ is the radius of gyration. $\Delta R_\theta$ is the Rayleigh ratio and corresponds to the macroscopic scattering cross-section; $d\Sigma/d\Omega$ is used to express the scattering intensity in SANS and SAXS. $K$ is the contrast factor given by

$$K = \frac{4\pi^2}{N_A\lambda_0^4}\left(n_{standard}\frac{dn}{dc}\right)^2 \quad (8)$$

It contains the Avogadro constant $N_A$, the wavelength of the laser in vacuo $\lambda_0$, the refractive index of the standard (in this case toluene) $n_{standard}$, and the refractive index increment of the polymer in the solvent $dn/dc$.

SLS data were corrected for the scattering from the solvent and normalized to absolute intensities by comparison to a toluene standard.

**Small-Angle Scattering Analysis.** The form factor fits of the small-angle scattering data were done using the SASET program.[44] Instrumental resolution for SANS has been taken into account according to ref 45. The form factor is convoluted with a resolution function $R(q,\sigma_q)$, which depends on wavelength spread, finite collimation of the beam, and detector resolution

$$P(q)_{smeared} = \int R(q, \sigma_q)P(q)dq \quad (9)$$

We took into account the instrumental resolution for all points from each detector configuration and merged the data only for final representation. This approach does not involve truncation of the data in the region of overlapping $q$, which leads to a larger number of available data points in the analysis.

**Scattering for Gaussian and Generalized Gaussian Chains.** The scattering of a Gaussian chain with a radius of gyration $R_g$ and a Flory exponent $\nu$ of 0.5 can be described by the Debye equation[46]

$$P(q) = \frac{2(\exp(-q^2R_g^2) - 1 + q^2R_g^2)}{(q^2R_g^2)^2} \quad (10)$$

In order to be able to describe the scattering from polymer chains where the Flory exponent is deviating from $\nu = 0.5$, the equation can be generalized to[47]

$$P(q) = \frac{1}{\nu U^{1/2\nu}}\gamma\left(\frac{1}{2\nu}, U\right) - \frac{1}{\nu U^{1/\nu}}\gamma\left(\frac{1}{\nu}, U\right) \quad (11)$$

with $U$ being defined as

$$U = (2\nu + 1)(2\nu + 2)\frac{q^2R_g^2}{6} \quad (12)$$

and $\gamma(a,x)$ being the incomplete Gamma function

$$\gamma(a, x) = \int_0^x t^{a-1}\exp(-t)dt \quad (13)$$

**Scattering from Block Copolymer Micelles with Self-Avoiding Chains in the Corona.** The form factor of self-assembled block copolymers with excluded volume interaction of the polymer chains was first treated by Pedersen.[48−51] The macroscopic scattering cross-section $d\Sigma/d\Omega(q)$ of a solution of block copolymer micelles can be written as[50]

$$\frac{d\Sigma}{d\Omega}(q) = N[N_{agg}^2\beta_{core}^2A_{core}^2(q) + N_{agg}\beta_{corona}^2P'_{corona}(q) + 2N_{agg}^2\beta_{core}\beta_{corona}A_{core}(q)A_{corona}(q) + N_{agg}(N_{agg} - P'_{corona}(0))\beta_{corona}^2A_{corona}^2(q)] \quad (14)$$

where $N$ is the number density of micelles, $N_{agg}$ is the aggregation number of micelles, $\beta_{core}$ and $\beta_{corona}$ are the total excess scattering length of the block forming the spherical core and the corona, respectively. They are defined as

$$\beta_{corona} = V_{m,corona}DP_{corona}\Delta\rho_{corona} \quad (15)$$

and

$$\beta_{core} = V_{m,core}DP_{core}\Delta\rho_{core} \quad (16)$$

with $V_m$ being the molecular volume of the respective monomer unit, $DP_{corona}$ and $DP_{core}$ are the degree of polymerization of the corona and core block, respectively, and $\Delta\rho$ is the corresponding excess scattering length density.

Equation 14 consists of four different contributions: scattering from the spherical and homogeneous core $A_{core}^2(q)$, scattering from the polymer chains in the corona $P'_{corona}(q)$, the cross-term between core and corona $A_{core}(q) \times A_{corona}(q)$, and the cross-term between different chains $A_{corona}^2(q)$. $A_{core}(q)$ is the scattering amplitude of a homogeneous sphere[52] with radius $R_{core}$

$$A_{core}(q) = 3\frac{\sin(qR_{core}) - qR_{core}\cos(qR_{core})}{(qR_{core})^3} \quad (17)$$

$P'_{corona}(q)$ is the form factor of a chain in the corona. It contains the self-correlation of the chain $P_{exv}(q)$ as well as the interaction between the chains, which is expressed by the interaction parameter $\nu$[50,53]

$$P'_{corona}(q) = \frac{P_{exv}(q)}{1 + \nu P_{exv}(q)} \quad (18)$$

where $P_{exv}(q)$ is the form factor of a semi flexible self-avoiding chain, which is characterized by a radius of gyration of the polymer chains in the corona $R_{g,corona}$. This form factor was first derived by Pedersen and Schurtenberger[54] and later corrected.[55] In experiments, $\nu$ typically adopts values between 0 and 8 and is related to the osmotic compressibility $\kappa$ by[50,53,56]

$$\kappa = 1 + \nu \quad (19)$$

$A_{corona}(q)$ is given by



DOI: 10.1021/acs.macromol.9b01924
Macromolecules 2019, 52, 8759−8770

$$A_{\text{corona}}(q) = \frac{\int \rho_{\text{corona}}(r) r^2 \frac{\sin(qr)}{qr} \mathrm{d}r}{\int \rho_{\text{corona}}(r) r^2 \, \mathrm{d}r} \tag{20}$$

with $\rho_{\text{corona}}(r)$ as the scattering length density profile in the corona. In this work, we use a Gaussian profile, which is defined as

$$\rho_{\text{corona}}(r) = \begin{cases} 0 & \text{for } r < R_{\text{core}} \\ 1 & \text{for } r = R_{\text{core}} \\ \exp\left(\frac{-(r - R_{\text{core}})^2}{2s^2}\right) & \text{for } r > R_{\text{core}} \end{cases} \tag{21}$$

with $s$ controlling the thickness of the corona.

In order to take into account the size distribution of micelles, we assumed a log-normal distribution of the aggregation number $N_{\text{agg}}$

$$p(N_{\text{agg}}) = \frac{1}{H\sqrt{2\pi}N_{\text{agg}}} \exp\left(\frac{-\log(N_{\text{agg}} - M)^2}{2H^2}\right) \tag{22}$$

where $H$ and $M$ define the distribution and are connected to the mean aggregation number $\overline{N_{\text{agg}}}$ and standard deviation $\sigma_{\overline{N_{\text{agg}}}}$ by

$$\overline{N_{\text{agg}}} = \exp\left(M + \frac{H^2}{2}\right) \tag{23}$$

$$\sigma_{\overline{N_{\text{agg}}}} = \sqrt{\exp(H^2 + 2M)(\exp(H^2) - 1)} \tag{24}$$

The macroscopic scattering cross-section is therefore

$$\frac{\mathrm{d}\Sigma}{\mathrm{d}\Omega}_{\text{polydisperse}}(q) = \int \frac{\mathrm{d}\Sigma}{\mathrm{d}\Omega}(q) p(N_{\text{agg}}) \mathrm{d}N_{\text{agg}} \tag{25}$$

**Isothermal Titration Calorimetry.** ITC measurements were performed using a VP-ITC from Malvern Instruments. Typically, the cell contained 1.4 mL of polymer solution, and the injection volumes were increased continuously during the titration ranging from 3 to 16 $\mu$L with a time span of 300 s in between the injections. In order to avoid the "first injection anomaly", a short down motion of the plunger was performed prior to insertion of the syringe into the active chamber.[57] The range of values of the $M^{2+}$/polymer ratios was extended by performing several titrations with changing concentration of earth alkaline metal cations.[58] The baseline correction and integration were performed using NITPITC.[59] We did not correct the signals for the heat of dilution of the polyelectrolyte and the metal cations because those contributions were considerably smaller than the heat of binding. The data were, if possible, fitted using the model of a single set of identical sites or two sets of independent sites. The details of the models are described in the Supporting Information.

## RESULTS AND DISCUSSION

**Solution Behavior.** We showed previously that aqueous solutions of PA-*b*-PSS block copolymers form spherical block copolymer micelles in the presence of $Ca^{2+}$. Because $Ca^{2+}$ shows a specific interaction with PA but not with PSS, $Ca^{2+}$ complexes the PA block and forms the core of the micelles, while PSS forms the corona. Furthermore, we demonstrated that micelle formation can be triggered for a sample in the single chain state by an increase of temperature because of the entropic nature of $Ca^{2+}$ binding to PA.[20]

The main focus of this work is to clarify if similar micelles can be found for the two other earth alkaline cations $Sr^{2+}$ and $Ba^{2+}$ and in particular, how temperature changes affect the binding of the multivalent cations to the block copolyelectrolyte. For the present work, we choose a polymer with a long PA block and a relatively short PSS block. In order to exploit the full potential of SANS, we use a block copolymer which contains a deuterated PA block. Deuteration allows us to match different parts of the polymer in neutron scattering by using mixtures of light and heavy water as a solvent.[60] The corresponding polymer is denoted as $d_3$-$PA_{1190}PSS_{70}$. In addition, we use an identical block copolymer with fully hydrogenated blocks, denoted as $h_3$-$PA_{1190}PSS_{70}$. Figure 1A

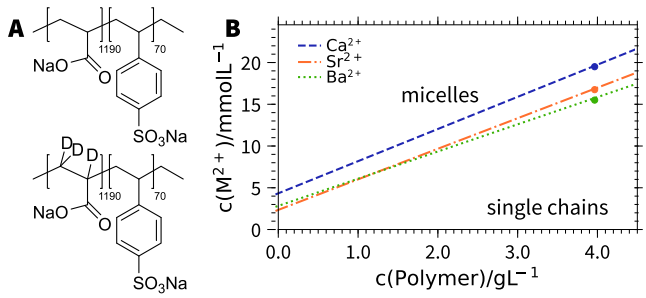


**Figure 1.** (A) Chemical structure of the block copolymers. (B) Simplified diagram of micelle formation with $d_3$-$PA_{1190}PSS_{70}$/$h_3$-$PA_{1190}PSS_{70}$ in the presence of $Ca^{2+}$, $Sr^{2+}$, and $Ba^{2+}$. The points indicate the compositions, where temperature-dependent SANS and light scattering experiments were performed. An extended version of the phase diagram can be found in the Supporting Information.

shows the chemical structure of the block copolymers, and Table 1 summarizes the molecular weights and hydrodynamic

**Table 1. Overview of Polymer Composition, Weight-Averaged Molecular Weight $M_w$, and Hydrodynamic Radius $R_h$ Determined from NMR and SLS and DLS in 100 mmol $L^{-1}$ NaCl and in the Absence of $M^{2+}$**

| sample | PA/PSS/mol %[a] | $M_w$/kg $mol^{-1}$[b] | $R_h$/nm[c] |
|---|---|---|---|
| $h_3$-$PA_{1190}PSS_{70}$ | 94/6 | 160 ± 2 | 13.8 ± 0.6 |
| $d_3$-$PA_{1190}PSS_{70}$ | 94/6 | 181 ± 3 | 13.6 ± 0.5 |

[a]Obtained by NMR. [b]Obtained by SLS. [c]Obtained by DLS.

radii from DLS/SLS as well as the ratio between PA and PSS of the block copolymers determined by NMR. Details of the characterization can be found in ref 20 and in the Supporting Information.

Figure 1B illustrates the solution behavior of $h_3$-$PA_{1190}PSS_{70}$/$d_3$-$PA_{1190}PSS_{70}$ in the presence of $Ca^{2+}$, $Sr^{2+}$, and $Ba^{2+}$ at room temperature. The boundaries for micelle formation with $h_3$-$PA_{1190}PSS_{70}$ and $d_3$-$PA_{1190}PSS_{70}$ are identical within the experimental accuracy. The block copolymer shows a solution behavior, which is similar to the one observed for PA homopolymers described by eq 1. This means that with increasing polymer concentration, the amount of $M^{2+}$ required to induce a phase transition increases. However, instead of precipitation as found for PA homopolymers,[25,61,62] the formation of stable micelles takes place in the case of block copolyelectrolytes.

In order to facilitate meaningful scattering experiments and suppress potential interparticular interferences by electrostatic screening, all experiments were performed in the presence of additional NaCl as an inert salt. Addition of NaCl was limited to accomplish an overall level of cationic charges of 0.1 M = $2[M^{2+}] + [Na^+]$. Variation of this level would have generated one further parameter to control the interactions[24,61] but was not applied in the present work to keep the complexity as low as possible.



DOI: 10.1021/acs.macromol.9b01924
Macromolecules 2019, 52, 8759−8770

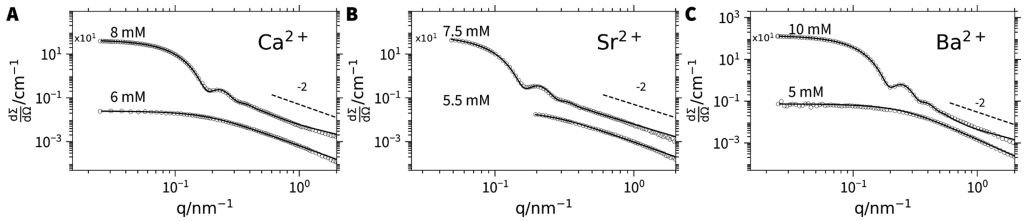


**Figure 2.** SAXS profiles of $h_3$-$PA_{1190}PSS_{70}$ ($c$ = 1 g $L^{-1}$) in the presence of different concentrations of $Ca^{2+}$ (A), $Sr^{2+}$ (B), and $Ba^{2+}$ (C). The solid lines represent fits to the model of the generalized Gaussian chain[47] or a spherical polydisperse block copolymer micelle.[48,50] Table 2 summarizes the results of the fits.

In order to investigate the structure of the micelles in the presence of $Ca^{2+}$, $Sr^{2+}$, and $Ba^{2+}$, we performed SAXS experiments of $h_3$-$PA_{1190}PSS_{70}$ in the micelle regime in the presence of the three cations. Figure 2 shows the corresponding SAXS profiles of a sample in the single-chain region and in the micelle region for all three cations, respectively.

The curve with the lowest concentration of $M^{2+}$ shows a slope close to −2 at high $q$. Upon increase of the $M^{2+}$ concentration, a dramatic increase of the forward scattering is observed together with the formation of well-defined minima in the scattering curves. This shows that block copolymer micelles are formed in the presence of all three cations.

The curves in the single-chain region can be well described by the model of a generalized Gaussian chain[47] with Table 2 summarizing the fit parameters. The resulting radii of gyration $R_{g,free}$ range between 6.3 and 8.2 nm. Moreover, we find Flory exponents $\nu$ between 0.4 and 0.5, which is close to the value of polymers in a $\theta$ solvent. We do not observe a structure factor, which implies that the charges of the polyelectrolytes are highly screened because of the large amount of salt present in solution.

**Table 2. Structural Parameters from the Form Factor Fits of the SAXS Data Shown in Figure 2**[a]

| | $Ca^{2+}$ | | $Sr^{2+}$ | | $Ba^{2+}$ | |
|---|---|---|---|---|---|---|
| $c(M^{2+})$/mM | 6 | 8 | 5.5 | 7.5 | 5 | 10 |
| $\phi_{micelles}$ | 0.0 | 0.79 | 0.0 | 0.73 | 0.0 | 1.0 |
| $R_{g,free}$/nm | 8.2 | 5.2 | 6.3 | 6.2 | 6.7 | |
| $\nu$ | 0.49 | 0.36 | 0.44 | 0.53 | 0.38 | |
| $R_{core}$/nm | | 22.8 | | 25.6 | | 21.6 |
| $\sigma_{R_{core}}/R_{core}$ | | 0.109 | | 0.104 | | 0.113 |
| $R_{g,corona}$/nm | | 0.7 | | 2.3 | | 1.0 |
| $f_{solvent}$ | | 0.83 | | 0.60 | | 0.90 |

[a]An extended version including errors of the fitting parameters can be found in the Supporting Information. Fits at the lower $c(M^{2+})$ were carried out with the model of generalized Gaussian chains[47] and fits at the higher $c(M^{2+})$ with the model of a spherical block copolymer micelle[20,48,50] or a mixture of block copolymers and free generalized Gaussian chains.

We used the previously suggested model of spherical block copolymer micelles,[20,48,50] consisting of a PA core complexed by the multivalent cation $M^{2+}$ and PSS chains in the corona to describe the data of the samples in the micelle region. This model has been shown to describe the situation for $Ca^{2+}$ and is expected to be similar for all three cations as the binding to PA is similar and the PA block is considerably longer than the PSS block. The fit parameters are summarized in Table 2. The scattering curves for the micelles formed in the presence of all three cations can be well described by the suggested model. The micelles have similar dimensions, consisting of a relatively large core formed of PA/$M^{2+}$ with a radius $R_{core}$ between 21.6 and 25.6 nm. The corona is formed by PSS and is rather thin with a radius of gyration of the polymers in the corona $R_{g,corona}$ between 0.7 and 2.3 nm. The overall micelles are rather monodisperse with polydispersities $\sigma_{R_{core}}/R_{core}$ close to 10%. By fitting the scattering data in absolute intensities, knowing the polymer concentration, scattering length densities, and block lengths, it turned out that the micelle cores contain a large volume fraction $f_{solvent}$ of water. $f_{solvent}$ is defined as

$$f_{solvent} = 1 - \frac{(V_{m,monomer\ unit} + 0.5V_{m,M^{2+}})DP_{core}N_{agg}}{\frac{4}{3}\pi R_{core}^{3}} \quad (26)$$

where $V_{m,monomer\ unit}$ is the molecular volume of one monomer unit of the core forming block, in this case PA, and $V_{m,M^{2+}}$ is the molecular volume of the corresponding divalent cation, $DP_{core}$ is the degree of polymerization of the core block, and $N_{agg}$ is the aggregation number. The high volume fractions of water found for the core of the micelles are in agreement with our previous contrast-variation study of PA-*b*-PSS in the presence of $Ca^{2+}$.[20]

For the micelles in the presence of $Ca^{2+}$ and $Sr^{2+}$, we had to take into account a small fraction of nonmicellized polymer chains ($\phi_{micelles}$ < 1.0).

Because $Ba^{2+}$ also interacts with the PSS block, we also tried a model with $Ba^{2+}$/PSS in the core of the micelles and PA in the corona. The polymer concentration, knowledge of block length, and the corresponding molar volumes of the blocks allowed us to heavily constrain the fit. This model was not able to describe the data sufficiently well and furthermore gave unreasonable values for the parameter $s$ controlling the corona thickness and the radius of gyration of the polymers in the corona $R_{g,corona}$. The best fit is shown in Figure S8 of the Supporting Information.

In short, we find spherical micelles with similar dimensions for $Ca^{2+}$, $Sr^{2+}$, and $Ba^{2+}$. The core of the micelles is formed by PA/$M^{2+}$ together with a high volume fraction of water. The corona of the micelles is formed by PSS. PA is complexed by the bivalent alkaline earth cations, and therefore, a microphase separation of the $M^{2+}$/PA blocks is taking place. The complex forms the core of the micelle and is highly swollen with water, typical for liquid−liquid phase transitions.[20,32] PSS forms the corona of the micelles and stabilizes the aggregates by charge repulsion.

**Temperature Effect on the Solution Behavior.** In order to study the effect of temperature on the self-assembly of the block copolymer in the presence of earth alkaline cations, we choose points in the phase diagram which are close to the



DOI: 10.1021/acs.macromol.9b01924
Macromolecules 2019, 52, 8759−8770

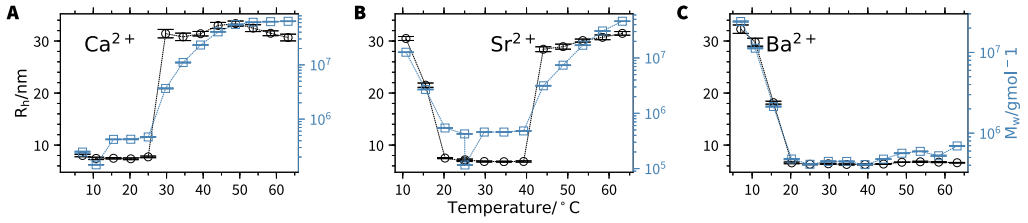


**Figure 3.** Hydrodynamic radius $R_h$ and apparent molecular weight $M_{w,app}$ of $d_3$-$PA_{1190}PSS_{70}$ in the presence of $Ca^{2+}$ (A), $Sr^{2+}$ (B) and $Ba^{2+}$ (C) as a function of temperature. The lines are guide to the eyes. The polymer concentration is 4g $L^{-1}$. The concentration of $M^{2+}$ is 19.5 mmol $L^{-1}$ ($Ca^{2+}$), 16.75 mmol $L^{-1}$ ($Sr^{2+}$), and 15.5 mmol $L^{-1}$ ($Ba^{2+}$). The solvent is composed of 25.2% $D_2O$.

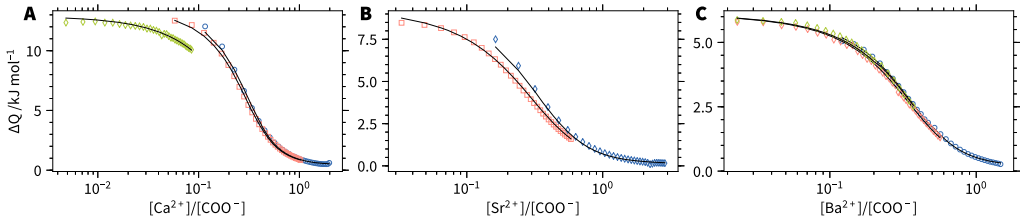


**Figure 4.** Isothermal titration curve of PA in the presence of $Ca^{2+}$ (A), $Sr^{2+}$ (B), and $Ba^{2+}$ (C). The curves show the heat of binding per injection as a function of the $M^{2+}$/PA ratio. We performed several titrations with varying concentrations of $M^{2+}$ to cover a large range of $M^{2+}$/PA. The solid lines are global fits with the model of a single set of identical binding sites. Details can be found in the Supporting Information. Table 3 summarizes the results.

single chain to micelle transition indicated as dots in Figure 1B. Because we also performed SANS measurements on those samples, we used the block copolymer $d_3$-$PA_{1190}PSS_{70}$. At room temperature, all of these samples are considered to be in the single-chain state. We performed temperature-dependent DLS and SLS on these samples. Figure 3 shows the hydrodynamic radii $R_h$ and the apparent molecular weight $M_{w,app}$ obtained from the temperature-dependent light scattering measurements.

Figure 3A shows the results for the block copolyelectrolyte in the presence of $Ca^{2+}$. The hydrodynamic radius at low temperatures (6−25 °C) is close to 8 nm, which we attribute to the presence of single chains of block copolymers in solution. Above 25 °C, $R_h$ increases to around 30 nm. Similarly, the apparent molecular weight $M_{w,app}$ increases from $4 \times 10^5$ to $6 \times 10^7$ g $mol^{-1}$. We attribute this strong increase to the formation of block copolymer micelles. It has been shown previously for PA homopolymers that an increase in temperature can be used to promote binding of $Ca^{2+}$ to the polyelectrolyte chain.[26] This results in a chain collapse and eventually in aggregation and precipitation of the polymer. As demonstrated in our previous work,[20] stronger binding of $Ca^{2+}$ to the PA block leads to microphase separation because of the same temperature-promoted binding of $Ca^{2+}$ to PA. A detailed analysis of the structure using small-angle neutron scattering confirming this feature is presented later. We performed temperature cycles with the same sample several times and found that the temperature-induced single-chain to micelle transition was reversible and highly reproducible.[20]

Figure 3B shows $R_h$ and $M_{w,app}$ as a function of temperature for the PA-*b*-PSS block copolymer in the presence of $Sr^{2+}$. Again, a hydrodynamic radius of around 8 nm and an apparent molecular weight of $4 \times 10^5$ g $mol^{-1}$ indicate the presence of single chains in solution at room temperature. Upon increase of the temperature above 40 °C, a strong increase of $R_h$ as well as $M_{w,app}$ occurs similar to the increase observed with $Ca^{2+}$ cations. However, at temperatures below 20 °C, $R_h$ and $M_{w,app}$ also increase. From this, we conclude that block copolymer micelles are formed at high as well as low temperatures with an intermediate region, where the polymers are present as single chains. A previous work already showed that an increase of temperature promotes the binding of $Ca^{2+}$ and $Sr^{2+}$ to PA because of the entropic nature of the complexation.[26] However, lowering the temperatures did not show a chain collapse or aggregation of PA homopolymers. Even though PSS does not show a precipitation threshold with $Sr^{2+}$ at room temperature, we hypothesize that the PSS block plays an important role in the formation of the micelles at low temperatures. In order to shed light onto the binding situation we will use SANS and ITC experiments.

Figure 3C shows the results for the block copolymer in the presence of $Ba^{2+}$. In contrast to the samples with $Ca^{2+}$, there is an increase in $R_h$ and $M_{w,app}$ at low temperatures comparable to the sample with $Sr^{2+}$. Both quantities show a value close to the typical value of single chains at 25 °C. From this, we conclude that micelles are formed at low temperatures, while at temperatures in the regime of 20 °C < $T$ < 40 °C, the sample contains single chains.

Figure S13 of the Supporting Information shows the hydrodynamic radius $R_h$ of $d_3$-$PA_{1190}PSS_{70}$ in the presence of $Sr^{2+}$ during several heating and cooling cycles between 10, 25, and 65 °C. Micelles are formed at low temperatures, return to single chains at room temperature, and reform at high temperatures. This demonstrates that the samples are in thermodynamic equilibrium and the temperature effect on the solution behavior is fully reversible.

**Thermodynamics of Cation Binding and Micelle Formation.** In order to gain further insights into the origin of the described temperature behavior, we used ITC to link the information we obtained from temperature-dependent light scattering with thermodynamic quantities. ITC allows us to measure the consumed or released heat upon addition of $M^{2+}$ to a solution of the polyelectrolyte for a given temperature. The measured heat can be attributed to the binding of the metal cation to the anionic moiety.



DOI: 10.1021/acs.macromol.9b01924
*Macromolecules* 2019, 52, 8759−8770

Table 3. Thermodynamic Data for the $M^{2+}$ Binding to PA and PSS from ITC at 25 °C

| polymer | $M^{2+}$ | $K$/L mol$^{-1}$ | $\Delta H$/kJ mol$^{-1}$ | $T\Delta S$/kJ mol$^{-1}$ | $\Delta G$/kJ mol$^{-1}$ | $n$ |
|---|---|---|---|---|---|---|
| PA | $Ca^{2+}$ | $5.60 \times 10^3 \pm 0.16 \times 10^3$ | 16.3 ± 0.2 | 37.7 ± 0.3 | −21.4 ± 0.1 | 0.264 ± 0.002 |
| PA | $Sr^{2+}$ | $3.68 \times 10^3 \pm 0.21 \times 10^3$ | 13.4 ± 0.4 | 33.8 ± 0.5 | −20.4 ± 0.1 | 0.266 ± 0.005 |
| PA | $Ba^{2+}$ | $4.99 \times 10^3 \pm 0.16 \times 10^3$ | 7.6 ± 0.1 | 26.2 ± 0.2 | −21.1 ± 0.1 | 0.321 ± 0.002 |
| PSS | $Ca^{2+}$ | $2.82 \times 10^2 \pm 0.19 \times 10^2$ | 4.3 ± 0.4 | 18.3 ± 0.6 | −14.0 ± 0.2 | 0.228 ± 0.016 |
| PSS | $Sr^{2+}$(I) | $5.13 \times 10^3 \pm 2.91 \times 10^3$ | 2.2 ± 0.2 | 19.0 ± 1.8 | −21.2 ± 1.4 | 0.187 ± 0.008 |
| | $Sr^{2+}$(II) | $4.27 \times 10^2 \pm 2.83 \times 10^2$ | −0.23 ± 0.61 | 14.8 ± 1.7 | −15.0 ± 1.6 | 2.156 ± 0.160 |

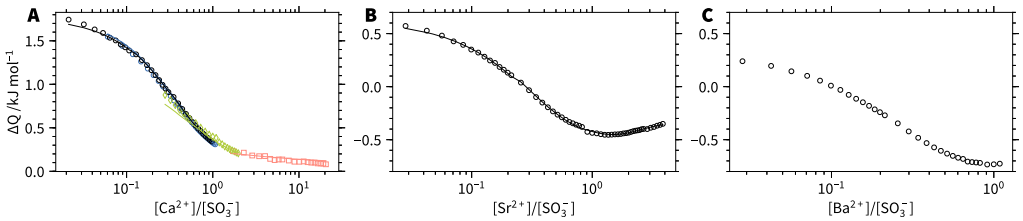


**Figure 5.** Isothermal titration curve of PSS in the presence of $Ca^{2+}$ (A), $Sr^{2+}$ (B), and $Ba^{2+}$ (C). The curves show the heat of binding per injection as a function of the $M^{2+}$/PA ratio. We performed several titrations for $Ca^{2+}$ with varying concentrations of the polymer to cover a large range of $Ca^{2+}$/PSS. The solid lines are global fits with the model of a single set of identical binding sites (A) and two sets of independent sites (B). Details can be found in the Supporting Information. Table 3 summarizes the results of the data analysis.

There are several driving forces for the binding of multivalent cations and micelle formation which have to be taken into account. The binding of multivalent cations to the anionic moiety results in a gain in entropy because two $Na^+$ are replaced by one $M^{2+}$. A release of water molecules from hydration shells also results in a gain of entropy. Equally important, the enthalpy of binding has to be taken into account.

In order to compare the contributions from the PA and PSS blocks, we performed ITC experiments on PA and PSS homopolymers in the presence of the three earth alkaline metal cations. Figure 4 shows the titration curves of PA with the three investigated earth alkaline metal cations at 25.0 °C. The heat of binding $\Delta Q$ is positive for all cations and follows a sigmoidal curve. This indicates that the binding of $M^{2+}$ to PA is an endothermic process. We performed several titrations with varying concentrations of $M^{2+}$ in the syringe to access a larger range of $M^{2+}$/PA. The data can be described by the model of a single set of identical binding sites, which is described in detail in the Supporting Information. All titrations for a given combination of $M^{2+}$ were analyzed globally using the same fitting parameters. Table 3 summarizes the results of the data analysis.

From the fits, we obtain the enthalpy of binding $\Delta H$, entropy of binding $\Delta S$, binding constant $K$, and the binding stoichiometry $n$. We find a positive binding enthalpy for all three cations demonstrating that the binding of $M^{2+}$ to PA is driven by entropy for all three metal cations. In a previous work[28] on PA and $Ca^{2+}$, this gain of entropy has been attributed to the release of two sodium cations as well as several water molecules upon binding. Compared to the previous work, we find slightly smaller binding enthalpies which we attribute to the presence of NaCl in our experiments compared to pure water. In fact, an increase in ionic strength in the solution leads to a decrease in $\Delta H$ for the binding of multivalent cations to DNA.[63] The binding enthalpy $\Delta H$ and along with it, the entropy of binding $\Delta S$ decreases according to $Ca^{2+} > Sr^{2+} > Ba^{2+}$. We attribute the decrease of $\Delta S$ when going from $Ca^{2+}$, $Sr^{2+}$, and $Ba^{2+}$ to a decreased amount of water released from hydration shells upon binding.

Next, we performed titration experiments for a PSS homopolymer in the presence of the three metal cations. Figure 5 shows the corresponding titration curves. For $Ca^{2+}$, the curves can be well described by the model of a single set of identical binding sites with a positive binding enthalpy. Compared to $Ca^{2+}$/PA, the binding enthalpy $\Delta H$, entropy $\Delta S$, and the binding constant $K$ are considerably smaller for $Ca^{2+}$/PSS. Table 3 summarizes the results from the data analysis. The smaller binding constant $K$ is in agreement with the macroscopic observation that there is no phase separation for PSS in the presence of $Ca^{2+}$.

Figure 5B shows the titration curve of $Sr^{2+}$/PSS. The curve differs considerably from the one found for $Ca^{2+}$/PSS. Clearly, there are two processes occurring upon addition of $Sr^{2+}$ to PSS: first, a binding process with a positive $\Delta H$ is taking place at low $Sr^{2+}$/PSS ratios. This is followed by a second process which has a negative $\Delta H$ contribution. Similarly, we find a two-step binding process for the titration of $Ba^{2+}$ to PSS, where again the first binding process has a positive $\Delta H$ contribution and the second process has a negative one.

A previous work[29] already revealed this two-step process for the $Ba^{2+}$/PSS system. In a first step, two $Na^+$ cations are replaced per $Ba^{2+}$ entering the polyelectrolyte domains, which results in a gain of entropy $\Delta S$ and a positive $\Delta H$ contribution. At higher $M^{2+}$/PSS ratios, the actual binding of the metal cation to the polyelectrolyte chain takes place as a second step with a negative $\Delta H$ term. From a qualitative comparison of the two curves in Figure 5B,C, it is obvious that this second contribution is weaker for $Sr^{2+}$ than for $Ba^{2+}$. This is in agreement with the macroscopic phase behavior. Whereas the system $Sr^{2+}$/PSS shows no precipitation threshold at 25 °C, $Ba^{2+}$/PSS does show one. We tried to fit the data with the model of two independent binding sites, which was successful for $Sr^{2+}$. However, for $Ba^{2+}$, using this model was not successful, which we mostly attribute to the smaller accessible $M^{2+}$/PSS range compared to $Sr^{2+}$ due to the precipitation of $Ba^{2+}$/PSS from solution at the end of the titration. This makes the data at high $Ba^{2+}$/PSS ratios unusable. The result of the fit for $Sr^{2+}$/PSS is summarized in Table 3. The obtained values confirm that two successive binding processes (I and II), one



DOI: 10.1021/acs.macromol.9b01924
Macromolecules 2019, 52, 8759−8770

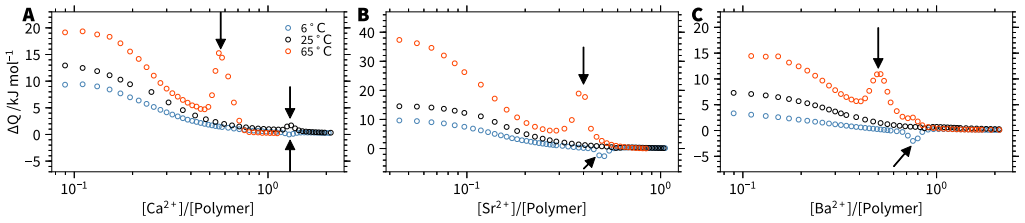


**Figure 6.** Isothermal titration curve of $h_3$-$PA_{1190}PSS_{70}$ in the presence of $Ca^{2+}$ (A), $Sr^{2+}$ (B), and $Ba^{2+}$ (C) at 6, 25, and 65 °C. The curves show the heat of binding per injection as a function of the $M^{2+}$/monomer unit ratio. Vertical Arrows denote micelle formation with PA cores and inclined arrows indicate $M^{2+}$ binding to PSS.

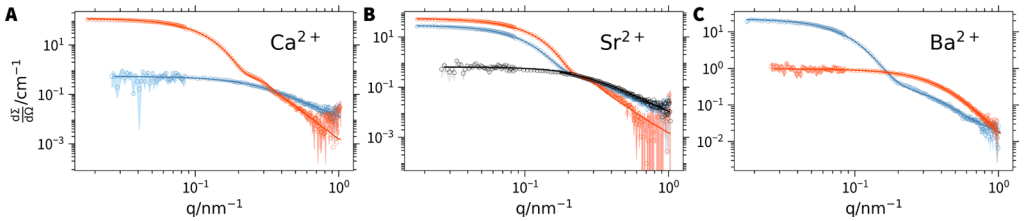


**Figure 7.** SANS profiles of $d_3$-$PA_{1190}PSS_{70}$ in the presence of $Ca^{2+}$, $Sr^{2+}$, and $Ba^{2+}$ at 8 °C (blue), 25 °C (black), and 65 °C (red). The solvent is composed of 25.2% $D_2O$. The samples are identical to the ones in Figure 3. The solid lines represent fits to the model of a generalized Gaussian chain[47] or block copolymer micelles.[48,50] Table 4 summarizes the resulting fit parameters.

with positive $\Delta H$ (I) and one with negative $\Delta H$ (II), occur. The same two successive binding processes occur with alkaline earth cations and PA. They are however more difficult to be discerned as both processes are endothermic.

After elucidating the effect of earth alkaline metal cations on the PA and PSS homopolymers, we performed ITC measurements on the $h_3$-$PA_{1190}PSS_{70}$ block copolymer system. As the length of the PA block is much longer than the length of the PSS block, we expect the ITC experiments to be dominated by the binding of $M^{2+}$ to the PA block. Figure 6A shows the titration curves with $Ca^{2+}$ at 6, 25, and 65 °C. The titration curves are composed of two parts: the first part, which shows that heat is consumed upon addition of $M^{2+}$, resembles the binding curves observed for $M^{2+}$ to PA. The second part consists of a peak at higher $M^{2+}$/polymer ratios. The peak at 25 °C corresponds to the sample composition, where micellization was observed (Figure 1B), which is also an endothermic process and hence driven by entropy. We marked the micellization peaks for all curves with a vertical arrow.

When decreasing the temperature, the heat consumed upon addition of $Ca^{2+}$ decreases, in agreement with the entropy-driven binding of $Ca^{2+}$ to PA. A decrease in temperature reduces the term $T\Delta S$ and consequently, $\Delta H$ becomes smaller in order to get similar values for the free energy $\Delta G$. Furthermore, when the temperature is lowered, the height of the micellization peak decreases. At 6 °C, the peak nearly disappears.

Figure 6B shows titration curves with $Sr^{2+}$ at 6, 25, and 65 °C. Similar to $Ca^{2+}$, the first part of the titration curve shows positive values for $\Delta Q$ and resembles the binding of $Sr^{2+}$ to PA. At higher $Sr^{2+}$/polymer ratios, we again observe a micellization peak. The same positive peak appears at 65 °C and disappears at 25 °C as observed in the case of $Ca^{2+}$. However, the titrations at 6 °C with $Sr^{2+}$ revealed a noticeable difference from the respective results observed in the presence of $Ca^{2+}$ as a small negative peak occurs at high $Sr^{2+}$/polymer ratios. The ITC experiments carried out with the PSS homopolymer and $Sr^{2+}$ suggest that the negative peak at 6 °C might arise from the second binding process of $Sr^{2+}$ to PSS which has a negative sign. Because the PSS block is considerably shorter than the PA block, the signal arising from binding of $Sr^{2+}$ is expected to be weak resulting in a very small contribution, which becomes more pronounced at low temperatures.

Figure 6C shows titration curves with $Ba^{2+}$ at 6, 25, and 65 °C. Again, we find a decrease of the initial values of $\Delta Q$ with decreasing temperature. Similar to $Sr^{2+}$, we find a positive peak at high temperatures and a negative peak at low temperatures. Applying the same argument used already for $Sr^{2+}$, we could expect the negative contribution arising from the second binding step of $Ba^{2+}$ to PSS.

A quantitative comparison of the titration curves of the block copolyelectrolytes with those of the respective homopolymers shown in Figure 5B,C also explains why the negative peak of the second process in the case of $Ba^{2+}$/PSS binding has a more negative $\Delta H$ term than the negative peak of the $Sr^{2+}$/PSS binding. Moreover, the binding enthalpy of $Ba^{2+}$/PA during the initial period of titration is smaller than the one for $Sr^{2+}$/PA.

We believe that a subtle balance of all these individual contributions results in the observed temperature behavior. We conclude that binding of $Sr^{2+}$ and $Ba^{2+}$ to the PSS block promotes the formation of micelles at low temperatures with PSS in the core because it makes the PSS block more hydrophobic, while the PA block becomes more hydrophilic.

**Invertible Micelles as Seen by SANS.** In order to get a more detailed insight into the structures of the micelles, we performed temperature-dependent SANS for the three samples discussed in Figure 3. The use of a deuterated PA block allowed us to match out the scattering from the PSS block. Accordingly, use of a mixture of 74.8% light and 25.2% heavy water as solvent results in a scattering contrast, where the scattering from $d_3$-PA is dominating, while the scattering from PSS is very weak. This facilitates the investigation of the micellar structure because the scattering patterns make it easy to distinguish between a model of PA forming the core or the corona. Figure 7 shows the SANS profiles for $d_3$-$PA_{1190}PSS_{70}$ in the presence of $Ca^{2+}$ (A), $Sr^{2+}$ (B), and $Ba^{2+}$ (C) at distinct temperatures. For all samples, we choose 8 and 65 °C as



DOI: 10.1021/acs.macromol.9b01924
Macromolecules 2019, 52, 8759−8770

Table 4. Structural Parameters from the Form Factor Fits of the SANS Data Shown in Figure 7 for $d_3$-$PAA_{1190}PSS_{70}$ in a Solvent Containing 25.2% $D_2O$[a]

| | $Ca^{2+}$ | | $Sr^{2+}$ | | | $Ba^{2+}$ | |
|---|---|---|---|---|---|---|---|
| temperature | 8 °C | 65 °C | 8 °C | 25 °C | 65 °C | 8 °C | 65 °C |
| $R_h$[b] | 8.0 | 30.7 | 30.5 | 7.2 | 31.5 | 29.8 | 6.6 |
| $R_g$[c] | 6.3 | 16.7 | 21.6 | 6.5 | 19.8 | 20.7 | 4.7 |
| $R_{g,free}$ | 6.9 | | | 6.7 | | | 5.0 |
| $\nu$ | 0.40 | | | 0.37 | | | 0.26 |
| micelle core | | $PA/Ca^{2+}$ | $PSS/Sr^{2+}$ | | $PA/Sr^{2+}$ | $PSS/Ba^{2+}$ | |
| $N_{agg}$ | | 145 | 38 | | 81 | 36 | |
| $R_{core}$ | | 17.6 | 7.0 | | 18.3 | 5.6 | |
| $\sigma_{R_{core}}/R_{core}$ | | 0.19 | 0.10 | | 0.17 | 0.02 | |
| $R_{g,corona}$ | | 1.0 | 9.8 | | 1.2 | 8.0 | |
| $f_{solvent}$ | | 0.650 | 0.669 | | 0.705 | 0.707 | |

[a]An extended version including error estimates can be found in the Supporting Information. [b]Obtained from DLS. [c]Obtained from Guinier analysis of the SANS data.

temperatures. For the sample with $Sr^{2+}$, we additionally performed a SANS measurement at 25 °C.

The blue curve in Figure 7A shows the SANS profile of $d_3$-$PA_{1190}PSS_{70}$ in the presence of $Ca^{2+}$ at 8 °C. The curve shows a slope close to −2 at high $q$ and has no distinct oscillations. The curve can be well described by the form factor of a generalized Gaussian chain[47] with a radius of gyration $R_{g,free}$ of 6.9 nm and a Flory exponent $\nu$ of 0.4. Table 4 summarizes the hydrodynamic radius from DLS and the $R_{g,free}$ and $\nu$ obtained from the form factor analysis of the SANS data. Hence, the block copolymers exist as single chains in solution at low temperatures in the presence of $Ca^{2+}$.

The red curve in Figure 7A shows the SANS profile at 65 °C. Compared to the curve at low temperatures, the forward scattering is higher and there is a characteristic oscillation at around $q$ = 0.22 $nm^{-1}$. At high $q$, we find a slope considerably steeper, indicating a compact morphology of the PA chains at high temperatures. From the Guinier analysis at low momentum transfer $q$, we obtain a radius of gyration of 16.7 nm. Based on this and the previous results,[20] we used the model of a polydisperse block copolymer micelle to describe the data.[48,50] This model assumes that PA complexed by $Ca^{2+}$ forms the core of the micelle, while the corona is formed by PSS. In order to get reliable results for the aggregation number and the structure, we heavily constrained the fit using the known block ratio, molar volumes, polymer concentration, and scattering length densities.[20] Details can be found in the Supporting Information. The red solid line in Figure 7A shows the best fit with this model. Table 4 summarizes the fit parameters. We obtain an aggregation number of 145 together with a core radius of 17.6 nm. Moreover, we find a radius of gyration for the PSS blocks in the corona of 1.0 ± 1.0 nm, which is close to the value we found in a previous study using the same polymer.[20] Recovery of this finite size for the value of $R_{g,corona}$ can be attributed to the fact that there is a slight mismatch of the scattering length density of the solvent. One also should keep in mind the large error bar of this parameter, which indeed shows that the scattering from the corona is very weak. In a previous work,[20] we investigated the micelle structure deep in the micelle regime in the presence of $Ca^{2+}$ at 25 °C. Compared to this previous work, the micelles formed with $Ca^{2+}$ at 65 °C (Figure 7A) contain a slightly lower amount of water. We attribute this lower water content to a larger amount of released water molecules from $PA/Ca^{2+}$. This is in agreement with the ITC measurements, which showed that the binding is driven by entropy which mainly arises from the release of water molecules, getting more pronounced at high temperatures.

Figure 7B shows SANS profiles of $d_3$-$PAA_{1190}PSS_{70}$ in the presence of $Sr^{2+}$ at a temperature of 8, 25, and 65 °C. The black curve shows the sample at 25 °C. The profile looks similar to the blue curve in Figure 7A recorded at 8 °C. From the Guinier analysis, we obtain a $R_g$ of 6.5 nm. The scattering curve can be well described by the model of a generalized Gaussian chain with a radius of gyration of 6.7 nm and a $\nu$ of 0.40. This nicely agrees with the results from temperature-dependent light scattering, where the sample at 25 °C was found to be in the single-chain region. Upon increase of the temperature to 65 °C, the scattering curve shows an increase of forward scattering. Moreover, a characteristic form factor oscillation becomes visible. We find a similar value of $R_g$ as for the $Ca^{2+}$ sample at 65 °C. From this, we conclude that micelles are formed. We employ the same model as used for the $Ca^{2+}$ sample to describe the scattering curve. The resulting aggregation number of 81 is close to the value estimated from static light scattering. In addition, a core radius of 18.3 nm and a value of $R_{g,corona}$ of 1.2 nm is obtained from the analysis. Similarly as for $Ca^{2+}$, the core is highly swollen by water. A micelle containing a $PA/Sr^{2+}$ core is in agreement with the results from ITC because high temperatures promote the entropy-driven binding of $Sr^{2+}$ to $COO^-$ of the acrylate groups.

The blue curve in Figure 7B shows the sample at a temperature of 8 °C. Again, the forward scattering increases quite dramatically with respect to the single-chain state at 25 °C. However, the high $q$ part of the scattering curves is nearly identical with the one of the single chains. This indicates that the conformation of the PA chains barely changes. Based on this observation and the results obtained from ITC, we tried to fit the data with two hypothetical models: one, which assumes that PA complexed by $Sr^{2+}$ forms the core of the micelle and PSS the corona and a second one with $PSS/Sr^{2+}$ in the core and PA in the corona. The fit was heavily constrained by knowing the molar volumes of the corresponding blocks, scattering length densities and the used polymer concentration. The model assuming a core of $PSS/Sr^{2+}$ yielded considerably lower values of $\chi^2$ than the one assuming $PA/Sr^{2+}$ to be in the core. The solid blue line in Figure 7B therefore shows the model based on $PSS/Sr^{2+}$ cores, whereas Figure S12 of the Supporting Information shows the best fit obtained with PA/



DOI: 10.1021/acs.macromol.9b01924
Macromolecules 2019, 52, 8759−8770

$Sr^{2+}$ in the core. Table 4 summarizes the fitting parameters. The micelles are formed by a rather small core of 7.0 nm formed by PSS/$Sr^{2+}$ and a considerable amount of water. The PA corona is rather large with $R_{g,corona}$ of 9.8 nm, which agrees with the fact that the PA block is rather long. The resulting overall dimension of the micelles is in good agreement with the hydrodynamic radius measured by DLS.

Figure 7C shows SANS profiles of the polymer sample in the presence of $Ba^{2+}$ at 8 and 65 °C. The sample at the high temperature can be well described by a generalized Gaussian[47] chain with a radius of gyration of 5.0 nm and $\nu$ of 0.26. This is in agreement with the result from DLS and SLS, from which we already expected the polymer to be present as a single chain. In contrast, the curve at 8 °C has a considerably larger forward scattering and shows a well-defined oscillation at $q$ = 0.19 $nm^{-1}$. Similarly as for the micelles formed at low temperatures in the presence of $Sr^{2+}$, there are two hypothetical models: PSS/$Ba^{2+}$ or PA/$Ba^{2+}$ forming the core of the micelle. Again, the model with a core formed by PSS/$Ba^{2+}$ describes the data considerably better and is shown as a solid blue line in Figure 7C. The alternative model of a PA/$Ba^{2+}$ core poorly describes the data and is shown in Figure S12 of the Supporting Information. The obtained micelle dimensions are similar to those of the sample in the presence of $Sr^{2+}$ at low temperatures. The PSS/$Ba^{2+}$ core is rather small with a radius of 5.6 nm, whereas the PA corona is rather thick with $R_{g,corona}$ of 8.0 nm.

We were surprised to not observe micelle formation in the presence of $Ba^{2+}$ at high temperatures as the binding of $Ba^{2+}$ to PA is also entropically driven. Therefore, another sample was prepared, this time even closer to the phase boundary. Figure S12 of the Supporting Information shows the temperature-dependent light scattering results of this sample. Similarly as before, micelle formation can be observed at low temperatures but this time also at high temperatures with an intermediate regime of single chains. However, the aggregation numbers and hydrodynamic radius for the micelles at high temperatures are considerably smaller as for $Sr^{2+}$ and $Ca^{2+}$. We attribute this to the considerably smaller entropy of binding $\Delta S$ for the combination PA/$Ba^{2+}$, making it harder to trigger the micellization by an increase of the temperature.

We performed similar SANS experiments with the completely hydrogenated polymer $h_3$-$PA_{1190}PSS_{70}$ in $D_2O$, which yielded identical temperature behaviors. However, the SANS data on this fully hydrogenated polymer, in particular of the samples with $Sr^{2+}$ and $Ba^{2+}$ at low temperatures, yield similar $\chi^2$ for the model with the PSS/$M^{2+}$ and the PA/$M^{2+}$ core. Thus, deuteration of one block is required to be able to differentiate between PA/$M^{2+}$ and PSS/$M^{2+}$ in the core of the micelles.

To sum up, we found two different temperature-dependent trends of $PA_{1190}PSS_{70}$ in the presence of earth alkaline cations. For all three cations, micelle formation can be triggered by increasing the temperature, arising from the strong endothermic binding to the PA block. Consequently, the micelles contain a core formed by PA/$M^{2+}$ and a corona formed by PSS. In contrast, micelle formation at low temperatures can only be observed for $Sr^{2+}$ and $Ba^{2+}$. This micelle formation at low temperatures arises from the exothermic binding of $M^{2+}$ to PSS and consequently leads to a micelle core formed by PSS/$M^{2+}$ and a corona formed by PA. As a result it is possible to generate an invertible micellar system with $Sr^{2+}$ and $Ba^{2+}$, which allows to change the core-forming block by a change in temperature.

## CONCLUSIONS

Polyelectrolytes exhibit ion-specific interactions with a large variety of metal cations. This ion specificity depends on the nature of the polyelectrolytes. $Ca^{2+}$, $Sr^{2+}$, and $Ba^{2+}$ as a representative set of bivalent alkaline earth cations interact specifically with the negative residues of sodium PAs.[25−27] The interaction is endothermic in nature due to the liberation of water molecules from solvation shells of the ionic residues.[28,29] Accordingly, addition of those cations to solutions of PA triggers separation of a polymer phase once a threshold of cation concentration is surpassed. An increase of temperature further promotes this phase separation. Unlike to PA, sodium PSS only interacts specifically with $Sr^{2+}$ and $Ba^{2+}$, and the interaction is exothermic in nature.[29−31] Now, the addition of $Sr^{2+}$ and $Ba^{2+}$ triggers phase separation with PSS which is further promoted by a decrease in temperature.

The present work makes use of these characteristic and differing interaction patterns in order to present a new route to micelle formation and its inversion by changing the temperature. The new route has been accomplished by combining the different patterns in a PA-*b*-PSS block copolyelectrolyte. As it turned out, the phase separation characteristic to the homopolyelectrolyte is confined to the respective micellar cores. The starting point is always a solution of the block copolyelectrolytes in their single coil state at a distinct concentration of alkaline earth cations low enough to not yet reach the threshold concentration but large enough to enable induction of micelle formation by a suitable change in temperature.

In the presence of $Ca^{2+}$, micelles are only formed via a temperature increase as this induces neutralization of the PA blocks by the specific bonding of $Ca^{2+}$ to the $COO^-$ residues.[20] The PA blocks form the core of the micelles, surrounded by stabilizing PSS blocks. With $Sr^{2+}$ and $Ba^{2+}$, the same types of micelles are generated by an increase of temperature. These micelles are also redissolved by decreasing the temperature, whereby the state of single coils is reached again. However, a further decrease in temperature generates a new type of micelle, now with PSS blocks in the core being neutralized by either $Sr^{2+}$ or $Ba^{2+}$ cations, respectively, and solubilized by dangling PA blocks. This establishes a complete inversion of micelles by a variation of temperature (Scheme 1). The process of micellar inversion could be unambiguously resolved by a combination of SANS with ITC. The morphological changes could be made visible by SANS on a polymer sample with one block of the copolyelectrolyte being fully deuterated. ITC reflected the heat changes accompanying the process of micellar inversion with micelle formation with PA/$M^{2+}$ cores at high temperatures unambiguously related to an endothermic

**Scheme 1. Illustration of the Temperature-Induced Micellization of PA-*b*-PSS in the Presence of $Ca^{2+}$, $Sr^{2+}$, and $Ba^{2+}$**

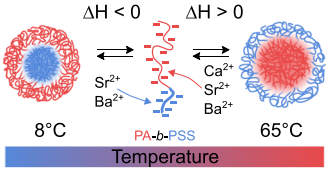




DOI: 10.1021/acs.macromol.9b01924
Macromolecules 2019, 52, 8759−8770

metal cation binding process and micelle formation with PSS/$M^{2+}$ cores at low temperatures to an exothermic metal binding process.

## ■ ASSOCIATED CONTENT

### Supporting Information

The Supporting Information is available free of charge on the ACS Publications website at DOI: 10.1021/acs.macromol.9b01924.

Additional data including an extensive overview of the fitting parameters with error bars, scattering length densities, measurements of the molar volume of PA and PSS, details regarding the ITC data analysis, description of the synthesis and characterization of all used polymers, reversibility of micelle formation, and $Ba^{2+}$-based inversion of micelles (PDF)

## ■ AUTHOR INFORMATION


### Corresponding Author

*E-mail: klaus.huber@upb.de.

### ORCID

Nico Carl: 0000-0002-9582-0356

Judith E. Houston: 0000-0001-5205-3620

Klaus Huber: 0000-0001-7512-206X


### Notes

The authors declare no competing financial interest.

## ■ ACKNOWLEDGMENTS

This work used the platforms of the Grenoble Instruct center (ISBG; UMS 3518 CNRS-CEA-UJF-EMBL) with support from FRISBI (ANR-10-INSB-05-02) and GRAL (ANR-10-LABX-49-01) within the Grenoble Partnership for Structural Biology (PSB). The authors thank the Institut Laue-Langevin (https://doi.ill.fr/10.5291/ILL-DATA.9-11-1910) and the European Synchrotron Radiation Facility for the provision of beam time. The authors gratefully acknowledge the financial support provided by JCNS to perform the neutron scattering measurements at the KWS2 instrument of the Heinz Maier-Leibnitz Zentrum (MLZ), Garching, Germany. The authors thank Aurel Radulescu for fruitful discussions and Caroline Mas for support with the ITC experiments and the Partnership for Soft Condensed Matter (PSCM) for supply of the light scattering. N.C. acknowledges funding for a PhD scholarship from Institut Laue-Langevin.

## ■ REFERENCES


(1) Zhang, L.; Eisenberg, A. Multiple Morphologies of "Crew-Cut" Aggregates of Polystyrene-b-poly(acrylic acid) Block Copolymers. *Science* **1995**, *268*, 1728−1731.

(2) Massey, J.; Power, K. N.; Manners, I.; Winnik, M. A. Self-assembly of a novel organometallic-inorganic block copolymer in solution and the solid state: Nonintrusive observation of novel wormlike poly(ferrocenyldimethylsilane)-b-Poly (dimethylsiloxane) micelles. *J. Am. Chem. Soc.* **1998**, *120*, 9533−9540.

(3) Du, J. Polymer Vesicles. *Advanced Hierarchical Nanostructured Materials*; John Wiley & Sons, Ltd, 2014; 9783527333, pp 177−192.

(4) Schilli, C. M.; Zhang, M.; Rizzardo, E.; Thang, S. H.; Chong, Y. K.; Edwards, K.; Karlsson, G.; Müller, A. H. E. A New Double-Responsive Block Copolymer Synthesized via RAFT Polymerization: Poly(N-isopropylacrylamide)-block-poly(acrylic acid). *Macromolecules* **2004**, *37*, 7861−7866.

(5) Lee, A. S.; Gast, A. P.; Bütün, V.; Armes, S. P. Characterizing the structure of pH dependent polyelectrolyte block copolymer micelles. *Macromolecules* **1999**, *32*, 4302−4310.

(6) Zhou, S.; Chu, B. Laser light scattering study of pressure-induced micellization of a diblock copolymer of poly(1,1-dihydroperfluorooctylacrylate) and poly(vinyl acetate) in supercritical carbon dioxide. *Macromolecules* **1998**, *31*, 5300−5308.

(7) Zhao, Y. Light-responsive block copolymer micelles. *Macromolecules* **2012**, *45*, 3647−3657.

(8) Ranka, M.; Katepalli, H.; Blankschtein, D.; Hatton, T. A. Schizophrenic Diblock-Copolymer-Functionalized Nanoparticles as Temperature-Responsive Pickering Emulsifiers. *Langmuir* **2017**, *33*, 13326−13331.

(9) Dompé, M.; Cedano-Serrano, F. J.; Heckert, O.; van den Heuvel, N.; van der Gucht, J.; Tran, Y.; Hourdet, D.; Creton, C.; Kamperman, M. Thermoresponsive Complex Coacervate-Based Underwater Adhesive. *Adv. Mater.* **2019**, *31*, 1808179.

(10) Kotsuchibashi, Y.; Ebara, M.; Aoyagi, T.; Narain, R. Recent advances in dual temperature responsive block copolymers and their potential as biomedical applications. *Polymers* **2016**, *8*, 380.

(11) Papadakis, C. M.; Müller-Buschbaum, P.; Laschewsky, A. Switch It Inside-Out: "Schizophrenic" Behavior of All Thermoresponsive UCST−LCST Diblock Copolymers. *Langmuir* **2019**, *35*, 9660.

(12) Bütün, V.; Liu, S.; Weaver, J. V. M.; Bories-Azeau, X.; Cai, Y.; Armes, S. P. A brief review of "schizophrenic" block copolymers. *React. Funct. Polym.* **2006**, *66*, 157−165.

(13) Feng, A.; Zhan, C.; Yan, Q.; Liu, B.; Yuan, J. A CO2- and temperature-switchable "schizophrenic" block copolymer: from vesicles to micelles. *Chem. Commun.* **2014**, *50*, 8958−8961.

(14) Wang, D.; Wu, T.; Wan, X.; Wang, X.; Liu, S. Purely salt-responsive micelle formation and inversion based on a novel schizophrenic sulfobetaine block copolymer: Structure and kinetics of micellization. *Langmuir* **2007**, *23*, 11866−11874.

(15) Vasantha, V. A.; Jana, S.; Lee, S. S.-C.; Lim, C.-S.; Teo, S. L.-M.; Parthiban, A.; Vancso, J. G. Dual hydrophilic and salt responsive schizophrenic block copolymers − synthesis and study of self-assembly behavior. *Polym. Chem.* **2015**, *6*, 599−606.

(16) Guragain, S.; Bastakoti, B. P.; Nakashima, K. Schizophrenic micellization of poly(ethylene oxide-b-methacrylic acid) induced by phosphate and calcium ions. *J. Colloid Interface Sci.* **2010**, *350*, 63−68.

(17) Vishnevetskaya, N. S.; Hildebrand, V.; Niebuur, B.-J.; Grillo, I.; Filippov, S. K.; Laschewsky, A.; Müller-Buschbaum, P.; Papadakis, C. M. "Schizophrenic" Micelles from Doubly Thermoresponsive Polysulfobetaine- b -poly(N -isopropylmethacrylamide) Diblock Copolymers. *Macromolecules* **2017**, *50*, 3985−3999.

(18) Vishnevetskaya, N. S.; Hildebrand, V.; Dyakonova, M. A.; Niebuur, B.-J.; Kyriakos, K.; Raftopoulos, K. N.; Di, Z.; Müller-Buschbaum, P.; Laschewsky, A.; Papadakis, C. M. Dual Orthogonal Switching of the "schizophrenic" Self-Assembly of Diblock Copolymers. *Macromolecules* **2018**, *51*, 2604−2614.

(19) Liu, S.; Billingham, N. C.; Armes, S. P. A schizophrenic water-soluble diblock copolymer. *Angew. Chem., Int. Ed.* **2001**, *40*, 2328−2331.

(20) Carl, N.; Prévost, S.; Schweins, R.; Huber, K. Ion-selective binding as a new trigger for micellization of block copolyelectrolytes with two anionic blocks. *Soft Matter* **2019**, *15*, 8266−8271.

(21) Yap, H. P.; Hao, X.; Tjipto, E.; Gudipati, C.; Quinn, J. F.; Davis, T. P.; Barner-Kowollik, C.; Stenzel, M. H.; Caruso, F. Synthesis, multilayer film assembly, and capsule formation of macromolecularly engineered acrylic acid and styrene sulfonate block copolymers. *Langmuir* **2008**, *24*, 8981−8990.

(22) Förster, S.; Hermsdorf, N.; Böttcher, C.; Lindner, P. Structure of polyelectrolyte block copolymer micelles. *Macromolecules* **2002**, *35*, 4096−4105.

(23) van der Maarel, J. R. C.; Groenewegen, W.; Egelhaaf, S. U.; Lapp, A. Salt-Induced Contraction of Polyelectrolyte Diblock Copolymer Micelles. *Langmuir* **2000**, *16*, 7510−7519.




DOI: 10.1021/acs.macromol.9b01924
*Macromolecules* 2019, 52, 8759−8770

(24) Hansch, M.; Hämisch, B.; Schweins, R.; Prévost, S.; Huber, K. Liquid-liquid phase separation in dilute solutions of poly(styrene sulfonate) with multivalent cations: Phase diagrams, chain morphology, and impact of temperature. *J. Chem. Phys.* **2018**, *148*, 014901.
(25) Schweins, R.; Goerigk, G.; Huber, K. Shrinking of anionic polyacrylate coils induced by Ca2+, Sr2+ and Ba2+: A combined light scattering and ASAXS study. *Eur. Phys. J. E* **2006**, *21*, 99−110.
(26) Lages, S.; Schweins, R.; Huber, K. Temperature-Induced Collapse of Alkaline Earth Cation-Polyacrylate Anion Complexes. *J. Phys. Chem. B* **2007**, *111*, 10431−10437.
(27) Huber, K. Calcium-induced shrinking of polyacrylate chains in aqueous solution. *J. Phys. Chem.* **1993**, *97*, 9825−9830.
(28) Sinn, C. G.; Dimova, R.; Antonietti, M. Isothermal Titration Calorimetry of the Polyelectrolyte/Water Interaction and Binding of $Ca^{2+}$: Effects Determining the Quality of Polymeric Scale Inhibitors. *Macromolecules* **2004**, *37*, 3444−3450.
(29) Hansch, M.; Kaub, H. P.; Deck, S.; Carl, N.; Huber, K. Reaction enthalpy from the binding of multivalent cations to anionic polyelectrolytes in dilute solutions. *J. Chem. Phys.* **2018**, *148*, 114906.
(30) Prabhu, V. M.; Muthukumar, M.; Wignall, G. D.; Melnichenko, Y. B. Dimensions of polyelectrolyte chains and concentration fluctuations in semidilute solutions of sodium−poly(styrene sulfonate) as measured by small-angle neutron scattering. *Polymer* **2001**, *42*, 8935−8946.
(31) Prabhu, V. M.; Muthukumar, M.; Wignall, G. D.; Melnichenko, Y. B. Polyelectrolyte chain dimensions and concentration fluctuations near phase boundaries. *J. Chem. Phys.* **2003**, *119*, 4085−4098.
(32) Lee, C.-L.; Muthukumar, M. Phase behavior of polyelectrolyte solutions with salt. *J. Chem. Phys.* **2009**, *130*, 024904.
(33) Kanai, S.; Muthukumar, M. Phase separation kinetics of polyelectrolyte solutions. *J. Chem. Phys.* **2007**, *127*, 244908.
(34) Zemb, T.; Lindner, P. *Neutrons, X-rays and Light: Scattering Methods Applied to Soft Condensed Matter*; North-Holland, 2002.
(35) Zentrum, H. M.-L. KWS-2: Small angle scattering diffractometer. *J. Large-Scale Res. Facil.* **2015**, *A29*, 2−6.
(36) Houston, J. E.; Brandl, G.; Drochner, M.; Kemmerling, G.; Engels, R.; Papagiannopoulos, A.; Sarter, M.; Stadler, A.; Radulescu, A. The high-intensity option of the SANS diffractometer KWS-2 at JCNS − characterization and performance of the new multi-megahertz detection system. *J. Appl. Crystallogr.* **2018**, *51*, 323−336.
(37) Orthaber, D.; Bergmann, A.; Glatter, O. SAXS experiments on absolute scale with Kratky systems using water as a secondary standard. *J. Appl. Crystallogr.* **2000**, *33*, 218−225.
(38) Boesecke, P. Reduction of two-dimensional small- and wide-angle X-ray scattering data. *J. Appl. Crystallogr.* **2007**, *40*, s423−s427.
(39) Frisken, B. J. Revisiting the method of cumulants for the analysis of dynamic light-scattering data. *Appl. Opt.* **2001**, *40*, 4087.
(40) Burchard, W.; Schmidt, M.; Stockmayer, W. H. Influence of Hydrodynamic Preaveraging on Quasi-Elastic Scattering from Flexible Linear and Star-Branched Macromolecules. *Macromolecules* **1980**, *13*, 580−587.
(41) Burchard, W.; Schmidt, M.; Stockmayer, W. H. Information on Polydispersity and Branching from Combined Quasi-Elastic and Intergrated Scattering. *Macromolecules* **1980**, *13*, 1265−1272.
(42) Cho, C. H.; Urquidi, J.; Singh, S.; Robinson, G. W. Thermal Offset Viscosities of Liquid H 2O, D 2O, and T 2O. *J. Phys. Chem. B* **1999**, *103*, 1991−1994.
(43) Zimm, B. H. The Scattering of Light and the Radial Distribution Function of High Polymer Solutions. *J. Chem. Phys.* **1948**, *16*, 1093−1099.
(44) Muthig, M.; Prévost, S.; Orglmeister, R.; Gradzielski, M. SASET: A program for series analysis of small-angle scattering data. *J. Appl. Crystallogr.* **2013**, *46*, 1187−1195.
(45) Pedersen, J. S.; Posselt, D.; Mortensen, K. Analytical treatment of the resolution function for small-angle scattering. *J. Appl. Crystallogr.* **1990**, *23*, 321−333.
(46) Debye, P. Molecular-weight determination by light scattering. *J. Phys. Colloid Chem.* **1947**, *51*, 18−32.
(47) Hammouda, B. SANS from Homogeneous Polymer Mixtures: A Unified Overview. *Polymer Characteristics*; Springer, 1993; Vol. *106*, pp 87−133.
(48) Pedersen, J. S.; Gerstenberg, M. C. Scattering Form Factor of Block Copolymer Micelles. *Macromolecules* **1996**, *29*, 1363−1365.
(49) Pedersen, J. S.; Svaneborg, C. Scattering from block copolymer micelles. *Curr. Opin. Colloid Interface Sci.* **2002**, *7*, 158−166.
(50) Svaneborg, C.; Pedersen, J. S. Form Factors of Block Copolymer Micelles with Excluded-Volume Interactions of the Corona Chains Determined by Monte Carlo Simulations. *Macromolecules* **2002**, *35*, 1028−1037.
(51) Pedersen, J. S.; Svaneborg, C.; Almdal, K.; Hamley, I. W.; Young, R. N. A Small-Angle Neutron and X-ray Contrast Variation Scattering Study of the Structure of Block Copolymer Micelles: Corona Shape and Excluded Volume Interactions. *Macromolecules* **2003**, *36*, 416−433.
(52) Rayleigh, L. Form factor of a homogenous sphere. *Proc. R. Soc. London, Ser. A* **1910**, *84*, 25−38.
(53) Svaneborg, C.; Pedersen, J. S. Block copolymer micelle coronas as quasi-two-dimensional dilute or semidilute polymer solutions. *Phys. Rev. E: Stat., Nonlinear, Soft Matter Phys.* **2001**, *64*, 010802.
(54) Pedersen, J. S.; Schurtenberger, P. Scattering Functions of Semiflexible Polymers with and without Excluded Volume Effects Excluded Volume Effects. *Macromolecules* **1996**, *29*, 7602−7612.
(55) Chen, W.-R.; Butler, P. D.; Magid, L. J. Incorporating intermicellar interactions in the fitting of SANS data from cationic wormlike micelles. *Langmuir* **2006**, *22*, 6539−6548.
(56) Sommer, C.; Pedersen, J. S.; Garamus, V. M. Structure and interactions of block copolymer micelles of brij 700 studied by combining small-angle X-ray and neutron scattering. *Langmuir* **2005**, *21*, 2137−2149.
(57) Mizoue, L. S.; Tellinghuisen, J. The role of backlash in the "first injection anomaly" in isothermal titration calorimetry. *Anal. Biochem.* **2004**, *326*, 125−127.
(58) Turnbull, W. B.; Daranas, A. H. On the Value of c: Can Low Affinity Systems Be Studied by Isothermal Titration Calorimetry? *J. Am. Chem. Soc.* **2003**, *125*, 14859−14866.
(59) Scheuermann, T. H.; Brautigam, C. A. High-precision, automated integration of multiple isothermal titration calorimetric thermograms: New features of NITPIC. *Methods* **2015**, *76*, 87−98.
(60) Stuhrmann, H. B. Neutron small-angle scattering of biological macromolecules in solution. *J. Appl. Crystallogr.* **1974**, *7*, 173−178.
(61) Schweins, R.; Huber, K. Collapse of sodium polyacrylate chains in calcium salt solutions. *Eur. Phys. J. E* **2001**, *5*, 117−126.
(62) Huber, K. Calcium-induced shrinking of polyacrylate chains in aqueous solution. *J. Phys. Chem.* **1993**, *97*, 9825−9830.
(63) Matulis, D.; Rouzina, I.; Bloomfield, V. A. Thermodynamics of DNA binding and condensation: isothermal titration calorimetry and electrostatic mechanism. *J. Mol. Biol.* **2000**, *296*, 1053−1063.



DOI: 10.1021/acs.macromol.9b01924
*Macromolecules* 2019, 52, 8759−8770